ELSEVIER

Computational Materials Science 16 (1999) 197–205

COMPUTATIONAL MATERIALS SCIENCE

Multiple scale meshfree methods for damage fracture and localization

Wing Kam Liu *, Su Hao, Ted Belytschko, ShaoFan Li, Chin Tang Chang

Department of Mechanical Engineering, The Technological Institute, Northwestern University, 2145 Sheridan Road, Evanston, IL 60208-3111, USA

Abstract

The Reproducing Kernel Particle Method (RKPM), which utilizes the fundamental notions of the convolution theorem, multiresolution analysis and meshfree properties, is reviewed. The multiple-scale RKPMs are then proposed as an alternative to commonly used numerical methods such as the finite element method. The elimination of a mesh, combined with the filtering properties of window functions, makes a particle method suitable for problems with large deformations, high gradients, and localization problems. This class of methods has been applied to shear band problems, and large deformation fracture and damage problems.

Keywords: Large deformation; Meshfree methods; Damage; Fracture; Localization; Finite element; Methods; Multiple scale; Shear band

1. Introduction

Recently, as an alternative and/or enhancement to the finite element method, there is a strong interest in the development of a new class of meshfree methods. The Smooth Particle Hydrodynamics (SPH) method is a grid-free computational method based on a Lagrangian formulation [11,12,32]. The continuum is represented by a set of particles eliminating the need for a mesh and consequently, alleviating mesh distortion problems. Based on a completely different approach, the element-free Galerkin method (EFG) developed by Belytschko et al. [3–5] applies moving least square interpolants to solve the problems of crack propagation and elasticity [2]. The recent developments, the Reproducing Kernel Particle Method (RKPM), proposed by Liu [22] and Liu et al. [28,29] included a boundary correction term to handle different boundary conditions, completeness conditions and error estimates.

The versatility of wavelets makes them very attractive in the discretization of differential equations. Glowinski et al. [13] explored the idea of using wavelets instead of piecewise polynomial trial functions in finite element methods (FEMs) type of methods. However, the straight use of wavelets as trial functions poses a number of difficulties. Low order wavelets cannot be employed due to the lack of regularity. The orthogonality of wavelets, as required in signal processing, is not important. Most significantly, the boundary conditions cannot be easily imposed in Dirichlet problems.

The shortcomings of the standard FEMs can be overcome through the application of particle-

* Corresponding author. Tel.: +1-847-491-7094; fax: +1-847-491-3915.

E-mail address: w-liu@nwu.edu (W.K. Liu).

0927-0256/99/$ - see front matter
PII: S0927-0256(99)00062-2

based methods, such as the RKPM. Wavelets exhibit attractive features in handling problems with various scales. These two ideas have been combined into the multiresolution RKPMs where the difficulties are alleviated by introducing a boundary correction function. The resolution of scales through multi-scale decomposition was introduced by Liu et al. [25–28,30,31]. This concept was later expanded into RKPM and has been applied in various fields such as structural acoustics [24,41], large deformation problems [20,26,7], computational fluid dynamics [14], micromechanics [37], and recently, large deformation fracture and damage problems [18] and shear bands [21].

The goal of this paper is to introduce the concepts involved in the development and use of RKPM, and show the effectiveness through several numerical applications. In Section 2, the fundamental notions in the development of the RKPMs such as the convolution theorem, multiresolution analysis and window functions are introduced. Section 3 is devoted to the mathematical formulation of the correction function. The need for a correction function is discussed, and the guidelines on its construction are given along with completeness conditions. A micromechanics damage model is discussed in Section 4. The formulation of RKPM in large deformation applications is introduced in Section 5. Several numerical examples are presented in Section 6.

2. Overview of multiple scale meshfree methods

2.1. Review

Both wavelet and SPH methods can be shown to belong to a class of reproducing kernel methods where the 'reproduced' function $u^R(x)$ is given by

$$u^R(x) = \int_{-\infty}^{+\infty} u(y)\phi(x-y)\,\mathrm{d}y. \tag{2.1}$$

Eq. (2.1) can be viewed as a projection operator. In Refs. [23,25,27,28,30], Liu and his coworkers showed that with the proper construction of a correction function to SPH, scaling functions, and wavelets, not only can artificial boundaries be eliminated, but the accuracy of discrete solutions can also be enhanced throughout the entire domain. Hence, Eq. (2.1) can be rewritten for a bounded domain as

$$u^R(x) = \int_\Omega u(y)C(x;x-y)\phi(x-y)\,\mathrm{d}y, \tag{2.2}$$

where $C(x;x-y)$ is the correction function and Ω is the computational domain. Using a flexible time–frequency/space–wave number analysis, as described in Section 3, we show how the correction function

$$C(x;x-y) = \beta_0(x) + \beta_1(x)(x-y) + \beta_2(x)(x-y)^2 + \cdots \tag{2.3}$$

not only compensates for the boundary-effect in finite domain function recovery, but also corrects the amplitude error caused by the conventional convolution theorem; in a discrete convolution, phase error can also be corrected.

Multiple scale analysis has its origin in signal analysis. Wavelet analysis is a contemporary science in image processing [8,9,38]. However, one major drawback in its application to computational mechanics is its inability to handle large deformation and complex domains. With the help of the correction function for the scaling functions and wavelets and the introduction of a dilation parameter a, we are able to perform multiresolution analysis of an arbitrary domain using only a set of nodes (or particles). The incorporation of this dilation parameter into the reproducing kernel Eq (2.2) gives

$$u^{R_a}(x) = \int_\Omega u(y)C_a(x;x-y)\phi_a(x-y)\,\mathrm{d}y = \int_\Omega u(y)\bar{\phi}_a(x-y)\,\mathrm{d}y. \tag{2.4}$$

One can view $\bar{\phi}_a(x)$ as a window function, so that the integral window transform of $\bar{\phi}_a(x)$ and $u(x)$, equivalent to the convolution, $\bar{\phi}_a * u(x)$, and denoted by $u^{R_a}(x)$, is a 'reproduction' of the original $u(x)$ with resolution of $\bar{\phi}_a(x)$. In other words, with the proper design of $\bar{\phi}_a(x)$, $u^{R_a}(x)$ will conserve all the resolutions and properties of the original solution $u(x)$ up to scale **a**. For this reason, we prefer to label $\bar{\phi}_a(x)$ and **a** as the scaling function and the

scaling (or refinement) parameter, respectively. A smaller **a** implies a finer scale solution of $u(x)$. In particular, when **a** approaches zero, $\bar{\phi}_a(x)$ approaches the Dirac delta function so that $\lim_{a\to 0} u^{R_a}(x) \to u(x)$.

3. Correction function

As indicated in Eq. (2.1), the solution to a differential equation or a set of differential equations can be expressed as

$$u^R(\mathbf{x}) = \int_{-\infty}^{+\infty} u(\mathbf{y})\phi(\mathbf{x};\mathbf{x}-\mathbf{y})\,\mathrm{d}\mathbf{y}, \tag{3.1}$$

where ϕ is a kernel function which acts like a filter or a reproducing kernel, and u^R is the reproduced solution of $u(\mathbf{x})$. In a finite domain, Eq. (3.1) can be written as

$$u^R(\mathbf{x}) = \int_{\Omega} u(\mathbf{y})\bar{\phi}(\mathbf{x};\mathbf{x}-\mathbf{y})\,\mathrm{d}\mathbf{y}, \tag{3.2}$$

where

$$\bar{\phi}(\mathbf{x};\mathbf{x}-\mathbf{y}) = C(\mathbf{x};\mathbf{x}-\mathbf{y})\phi(\mathbf{x}-\mathbf{y}). \tag{3.3}$$

The correction function, $C(\mathbf{x};\mathbf{x}-\mathbf{y})$, can be constructed in such a way to avoid the difficulties mentioned above. Since the integral defined in Eq. (3.2) is too complicated to be carried out analytically, it is generally discretized either by a set of particles. The methods involving mesh-free Lagrangian particles concerned with the solution of Eq. (3.2) are referred to as RKPMs. The construction of an appropriate correction function to compensate for the boundary effects and to minimize the amplitude and phase errors is as follows:

$$\begin{aligned}\bar{\phi}(\mathbf{x};\mathbf{x}-\mathbf{y}) &= C(\mathbf{x};\mathbf{x}-\mathbf{y})\phi(\mathbf{x}-\mathbf{y}) \\ &= \sum_{k=0}^{n} \beta_k(\mathbf{x})(\mathbf{x}-\mathbf{y})^k\phi(\mathbf{x}-\mathbf{y}).\end{aligned} \tag{3.4}$$

The numerical moments of window function $\phi(\mathbf{x})$ are defined as

$$m_k(\mathbf{x}) = \int_{\Omega} (\mathbf{x}-\mathbf{y})^k\phi(\mathbf{x}-\mathbf{y})\,\mathrm{d}\mathbf{y}, \quad k = 0,1,2,\ldots,n. \tag{3.5}$$

The unknown constants β's are determined by imposing the reproducing conditions:

$$\bar{m}_\alpha(\mathbf{a},\mathbf{x}) = \delta_{\alpha 0}, \quad 0 \leqslant |\alpha| \leqslant n. \tag{3.6}$$

It is noted that *multi-index notation* is applied for α to simplify the notation for multiple dimension. Enforcing the reproducing conditions, Eq. (3.6), on the modified window function, $\bar{\phi}$, yields

$$\mathbf{M}\beta = \mathrm{P}(0) \quad \text{or} \quad \beta = \mathbf{M}^{-1}\mathrm{P}(0), \tag{3.7}$$

where the components of the moment matrix **M** are

$$\begin{aligned}\mathbf{M}_i = \int_{\Omega} &(\mathbf{x}-\mathbf{y})^\alpha\phi_a(\mathbf{x};\mathbf{x}-\mathbf{y}) \\ &\times (\mathbf{x}-\mathbf{y})^\beta\,\mathrm{d}\mathbf{y}, \quad 0 \leqslant \alpha+\beta = i \leqslant n\end{aligned} \tag{3.8}$$

and P is the basis function defined as

$$\mathrm{P}(\mathbf{x}-\mathbf{y}) = [1,(\mathbf{x}-\mathbf{y}),\ldots,(\mathbf{x}-\mathbf{y})^n]^{\mathrm{T}}$$

and $\mathrm{P}(0) = [1,0,\cdots,0]^{\mathrm{T}}$.

4. Damage models

In this section, we briefly discuss the material model for void-containing ductile solids. Based on the cell model concept suggested by Rice and Tracey [35], Gurson [15] has derived the upper bound solutions for cylindrical cells and spherical cells with/without rigid inclusion:

$$\begin{aligned}\Phi_{\mathrm{GTN}} = &\left(\frac{\sigma_{\mathrm{eq}}}{\sigma_y}\right)^2 + 2q_1 f\cosh\left(\frac{3q_2\sigma_m}{2\sigma_y}\right) \\ &- (1+q_3 f^2) = 0,\end{aligned} \tag{4.1}$$

where σ_m, σ_{eq} and σ_y are the hydrostatic stress, the equivalent stress and the equivalent tensile flow stress representing the microscopic stress state in the matrix material, respectively. The constants q_1, q_2 and q_3 are introduced [34,39] in an attempt to make Gurson's equations agree with numerical studies of materials containing periodically distributed circular cylindrical voids and f is the current void volume fraction.

Another computational methodology of a micromechanics cell model is proposed to establish the constitutive law during material fracture which we

labeled as the HLC model [18]. When a damaged ductile material yields, $\Phi_{\mathrm{HLC}} = 0$. That is

$$\Phi_{\mathrm{HLC}}\left(\frac{\sigma_{\mathrm{eq}}}{\sigma_y}, \frac{\sigma_m}{\sigma_y}, f\right) = \left(\frac{\sigma_{\mathrm{eq}}}{\sigma_y}\right)^2 + \left(1 + \frac{1}{m_{20}}\right) f m_1 \exp\left(\frac{3\sigma_m}{2\sigma_y}\right) - 1 = 0, \tag{4.2}$$

where m_1 is a given material constant and the model parameter function m_{20} can be obtained based on computational cell modeling technique and no additional undetermined constants are required.

Various of applications of Gurson model and HLC model can be found in the fields of metal forming, fracture toughness simulation, and structure integrity analysis [18,6,36,16]. The HLC model, in conjunction with Meshless method, is very effective for simulating the large deformation processes during metal forming, penetration and ductile fracture.

5. RKPM formulations for large deformation

For large deformation problems, meshfree methods such as RKPM may, similar to the finite element method, be regarded as an updated Lagrangian method or a total Lagrangian method. As stated in [7,20], the total Lagrangian formulation requires more storage than the updated Lagrangian formulation in order to save the values of the shape functions and their derivatives. In contrast, the updated Lagrangian formulation requires the repeated searching and calculation of shape functions at each time step which often ruins computational efficiency. Thus, for transient problems with large deformations which will be considered in this work, the total Lagrangian formulation is desirable, since its computational cost is anticipated to be several orders of magnitude less than an updated Lagrangian formulation.

Consider a body which occupies a region Ω_X with boundary Γ_X at time $t = 0$ and is deformed to occupy a region Ω_x with deformed boundary Γ_x at time t. The motion of the continuum body is defined as

$$\mathbf{x} = \mathbf{X} + \mathbf{u}(\mathbf{X}, t), \tag{5.1}$$

where $\mathbf{X}$, $\mathbf{x}$, and $\mathbf{u}(\mathbf{X}, t)$ are the material coordinates, current spatial coordinates, and the displacement, respectively. For the total Lagrangian formulation, the governing equations may be stated as:

1. *Conservation of mass*:

$$\rho_0 = \rho J, \tag{5.2}$$

where J is the determinant of the deformation gradient $\mathbf{F}$, i.e., $J = |F| = |\partial \mathbf{x}/\partial \mathbf{X}|$.

2. *Equation of motion*:

$$\rho_0 \ddot{\mathbf{u}} = \nabla \cdot \mathbf{P} + \rho_0 \mathbf{b} \quad \text{or} \quad \frac{\partial P_{ji}}{\partial X_j} + \rho_0 b_i = \rho_0 \ddot{u}_i, \tag{5.3}$$

where $\mathbf{P}$ is the first Piola–Kirchhoff stress tensor and $\mathbf{b}$ is the vector of body force per volume.

3. *Constitutive laws*: For the modeling of hyperelastic materials, the second Piola–Kirchhoff stress $\mathbf{S}$ is calculated from the strain energy density function W, i.e, $S_{ij} = \partial W/\partial E_{ij}$ where $\mathbf{E}$ is the Green strain tensor.

4. *Boundary conditions*:

$$u_i = \bar{u}_i \quad \text{on } \Gamma_X^u, \tag{5.4}$$

$$n_j^0 P_{ji} = \bar{t}_i^0 \quad \text{on } \Gamma_X^t, \tag{5.5}$$

where $\Gamma_X^u \cup \Gamma_X^t = \Gamma_X$ and $\Gamma_X^u \cap \Gamma_X^t = \emptyset$.

With the RKPM interpolation functions and its derivatives as

$$u_i(\mathbf{X}, t) = \sum_{I=1}^{NP} N_I(\mathbf{X}) d_{Ii}(t)$$

and

$$u_{i,j}(\mathbf{X}, t) = \sum_{I=1}^{NP} \frac{\partial N_I(\mathbf{X})}{\partial X_j} d_{Ii}(t) \tag{5.6}$$

the discretized weak form of the momentum equation is obtained as

$$\mathbf{M}\ddot{\mathbf{d}} = \mathbf{f}^{\mathrm{ext}} - \mathbf{f}^{\mathrm{int}}, \tag{5.7}$$

where $\mathbf{M}$ is the lumped mass matrix, $\mathbf{f}^{\text{int}}$ is the internal force vector, and $\mathbf{f}^{\text{ext}}$ is the external force vector, respectively. It is noted that for total Lagrangian formulations, all the integrations above are performed over the material space Ω_X or surface Γ_X which are fixed during the time integration procedure.

6. Numerical examples

In this section, several numerical studies are presented including large deformation fracture, compression of a hyperelastic block, tension test of an elasto-viscoplastic tensile bar, and simulation of the John–Shah notched concrete beam to demonstrate the performance of RKPM.

6.1. Large deformation fracture

In this section, the deformation process and shear bands in a notch-bend specimen are studied. The setup of a plane-strain notch-bend specimen is shown in Fig. 1a. The geometrical parameters are $a : W : L = 1 : 2 : 8$ with $a = 0.0762$ (m). The deformation processes are considered to be quasi-static.

In the analysis, the visco-plastic strain hardening law suggested in [34] has been applied with the material constants are as follows: Young's modulus $E = 210$ GPa, $\sigma_0 = 470$ MPa, Poisson's ratio $v = 0.3$, the strain hardening exponent $N = 0.001$, and the reference strain rate $\dot{\epsilon}_0 = 0.00218$ with the strain rate exponent $m = 0.001$. The initial void volume fraction $f_0 = 0$ and the volume fraction of second material phase for void nucleation is 0.001.

In the numerical simulation, the specimen is modeled by 5504 RKPM particles. The deformation sequence at different time steps is shown in Fig. 1b. Note that in the computation, only the contact condition between the specimen and the punch at the original configuration has been taken into account.

To demonstrate the localized deformation around the crack tip and ligament clearly, a close-up of the deformed RKPM particles at the crack tip-ligament area of the specimen is shown in Fig. 1c. The comparison between particle (meshfree) and mesh-based methods is also presented. As shown in Fig. 1c, the mesh-based analysis will fail at the final deformation since it leads to a severe mesh distortion. On the contrary, the RKPM computation ran continuously until the right and the left parts of the specimen overlap with each other. This example demonstrates that particle-based numerical methods such as RKPM are not sensitive to mesh distortion.

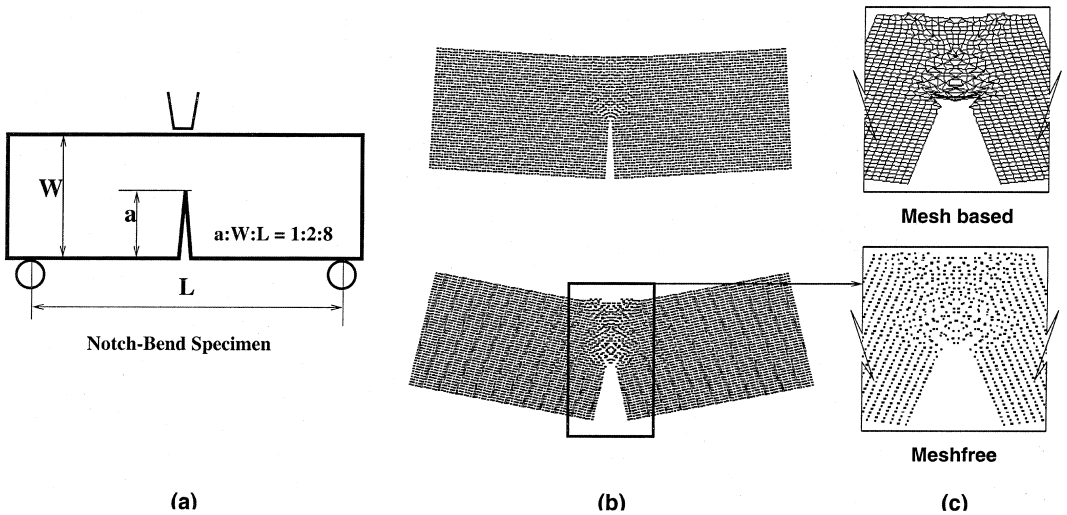

Fig. 1. Large deformation of a notch-bend specimen with ductile tearing fracture at the crack tip.

6.2. Compression of a hyperelastic block

In this section, a hyperelastic block under compression in plane strain is studied. The problem statement is sketched in Fig. 2. The modified Moony–Rivlin constitutive model [10] has been applied with the material constants: $\rho = 2.045 \times 10^{-3}$ (kg/m^3), $C_1 = 0.1265$ (MPa), $C_2 = 0.1012$ (MPa), and $\lambda = 0.1012 \times 10^3$ (GPa). The domain is discretized into 51×51 RKPM particles and the bilinear base functions are used. The constant time step increment is chosen as $\Delta t = 1 \times 10^{-6}$ (s).

The deformed shapes at several time stages are shown in Fig. 2. Finite element analysis is also performed with the mesh of 50×50, 4-node elements. The results are also shown in Fig. 2. The FEM analysis failed due to severe mesh distortion when the compression percentage reached 66%. RKPM computation, however, reached 90% compression with the help of the variable Δt. One of the strategies to determine Δt is given as follows:

$$\Delta t = \begin{cases} \Delta t_0 & \% \text{ of compression } \leqslant 50\% \\ \Delta t_0/2 & 50\% \leqslant \% \text{ of compression } \leqslant 75\%, \\ \Delta t_0/4 & \% \text{ of compression } \geqslant 75\% \end{cases}$$

where $\Delta t_0 = 1 \times 10^{-6}$ (s). Without mesh connectivity, it is shown that around 20 particles had been lift off from the surface of the block in 90% compression of RKPM computation.

6.3. Tension test of an elasto-viscoplastic tensile bar

In this example, the meshless hierarchical basis is used to simulate shear-band in an elasto-viscoplastic material. This problem has extensive engineering applications [1,33,40]. In this work, the wavelet adaptive algorithm is utilized to capture the localization mode [21]. The orientation of the wavelet basis is isotropic in space, and the enhancement of the numerical solutions due to wavelet basis comes out naturally as the outcome of numerical computation, though the adaptive regions are selected by a given criterion.

The model problem considered is the following tension test of an elasto-viscoplastic tensile bar, a rectangular specimen under plane strain tension. The prescribed displacement/velocity boundary condition is imposed at the both ends of the tensile bar as shown in Fig. 3. A power-law governed elasto-viscoplatic material is used in numerical computation, which is simular to those, e.g., [33]. In order to initiate shear bands the imperfectio is implanted, as introduced in [33].

In the example, both geometric imperfection as well as yield stress reduction are implanted and 3321 particles are used. An intuitive adaptive criterion is adopted: we refine the regions, or the set of particles, that have the highest accumulated viscoplastic strain distribution. The wavelet basis are added to 241 particles, which have the highest values of viscoplastic strain; subsequently, 482, or

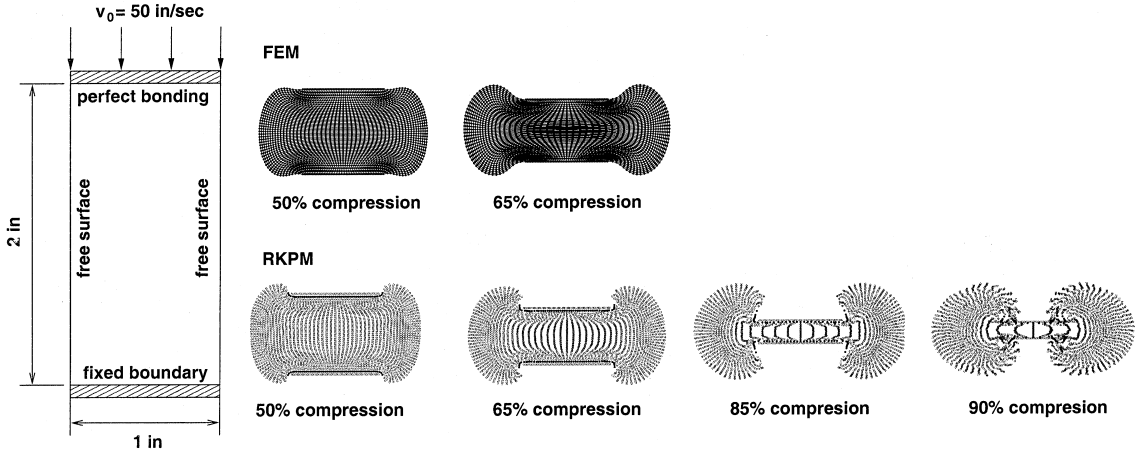

Fig. 2. Compression of a hyperelastic block.

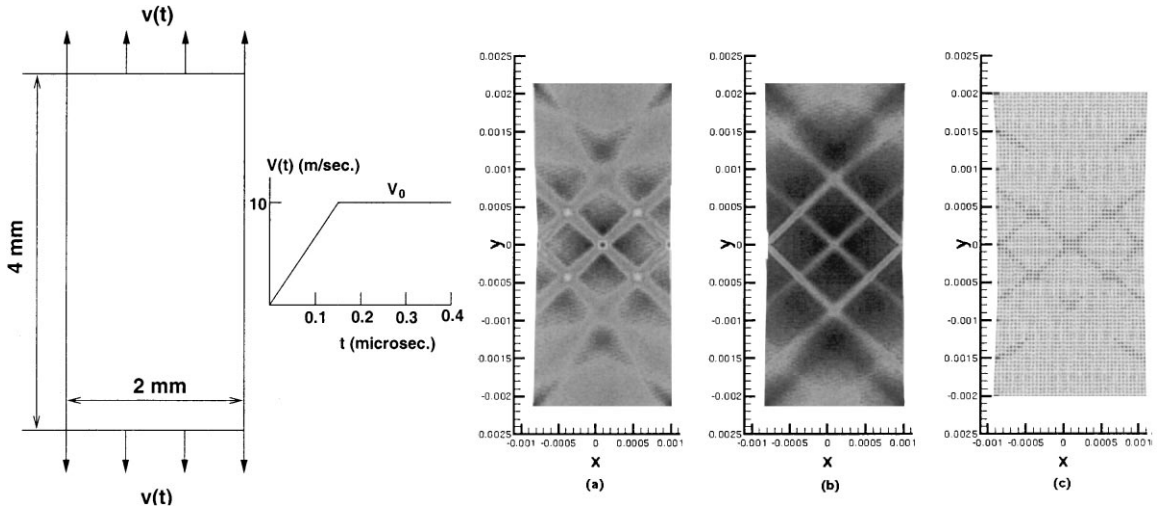

Fig. 3. The contours of the viscoplastic strain in the tensile bar: (a) without wavelet adaptivity; (b) with wavelet adaptivity; (c) the adaptivity pattern in undeformed configuration.

723, new degrees of freedom are adding into the primary shape function basis.

As shown in Fig. 3, one can observe that the width of the shear bands obtained from the wavelet adaptive solutions become thinner than the numerical solution without adaptivity.

6.4. Simulation of the John and Shah notched concrete beam

This problem has been investigated by EFG using linear elastic fracture mechanics. Based on the methodology of meshfree analysis and the

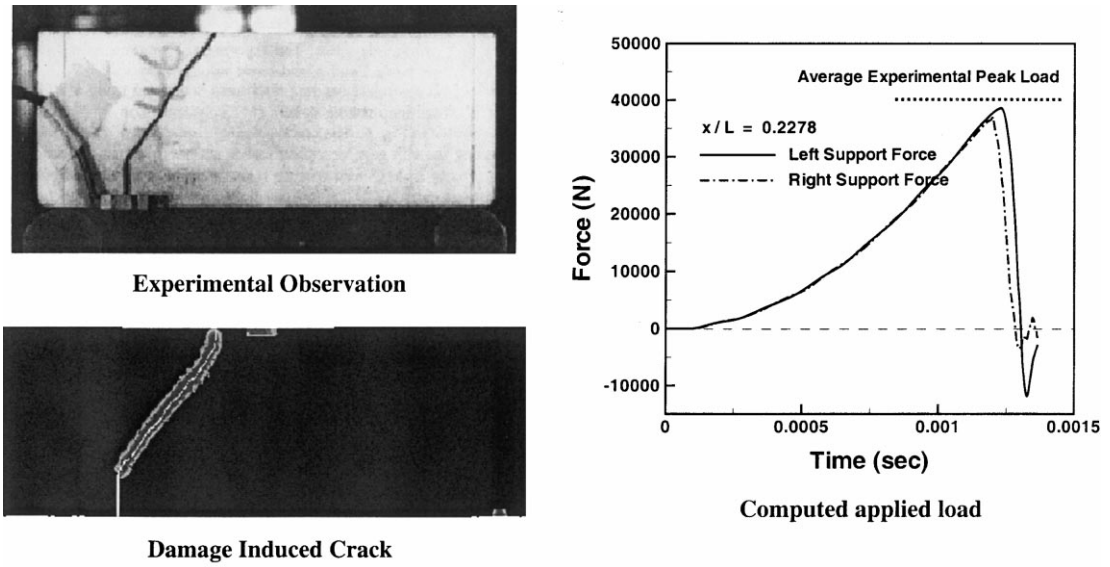

Fig. 4. Simulation of the John–Shah notched concrete beam.

visibility principle [3], the concept of 'damage induced cracking', the corresponding crack tip smoothing technique, and the computational meshfree algorithm have been developed [17]. As an applicational example, a dynamic crack growth process in a notched concrete bar has been analyzed using damage induced crack technique and meshless method.

As shown in Fig. 4, the bar to be studied is under dynamically three points bending, in which there is a premanufactured notch located away from the middle symmetric axis. Thus, the notch tip locally is under mixed mode I and mode II loading condition. This kind of specimen has been investigated experimentally by John and Shah [19]. The modified smooth cap model coupling damage has been applied to describe the constitutive behavior in conjunction with damage evolution. The simulated crack growth path and the support force as well as the comparison to experimental result are depicted in Fig. 4. The comparisons with linear elastic fracture EFG and experimental results are in good agreement.

Acknowledgements

The support of this research by Air Force Office of Scientific Research (AFOSR), Army Research Office (ARO), National Science Foundation (NSF) and Office of Naval Research (ONR) to Northwestern University is gratefully acknowledged. Sponsored in part by the Army High Performance Computing Research Center (AHPCRC) under the auspices of the Department of the Army Research Laboratory. The content does not necessarily reflect the position or the policy of the government, and no official endorsement should be inferred.

References

[1] T. Belytschko, H.-Y. Chiang, E. Plaskacz, High resolution two-dimensional shear band computations: imperfections and mesh dependence, Comput. Meth. Appl. Mech. Eng. (1994) 1–15.

[2] T. Belytschko, L. Gu, Y.Y. Lu, Fracture and crack growth by EFG methods, Modeling Simulation Mater. Sci. 2 (1994) 519–534.

[3] T. Belytschko, Y. Krongauz, D. Organ, M. Fleming, P. Krysl, Meshless methods: an overview and recent developments, Comput. Meth. Appl. Mech. Eng. 139 (1996) 3–47.

[4] T. Belytschko, Y.Y. Lu, L. Gu, Element free Galerkin methods, Int. J. Numer. Meth. Eng. 37 (1994) 229–256.

[5] T. Belytschko, Y.Y. Lu, L. Gu, A new implementation of the element free Galerkin method, Comput. Meth. Appl. Mech. Eng. 113 (1994) 397–414.

[6] C.T. Chang, The reproducing kernel particle method and its applications, Ph.D. Dissertation, Northwestern University, 1998.

[7] J.S. Chen, C. Pan, W.K. Liu, Reproducing kernel particle methods for large deformation analysis of nonlinear structures, Comput. Meth. Appl. Mech. Eng. 139 (1996) 195–228.

[8] C.K. Chui, An Introduction to Wavelets, Academic Press, New York, 1992.

[9] Daubechies, Ten Lectures on Wavelets, CBMS/NSF Series in Applied Mathematics, No. 61, SIAM Publication, 1992.

[10] I. Fried, A.R. Johnson, A note on elastic energy density function for largely deformed compressible rubber solids, Comput. Meth. Appl. Mech. Eng. 69 (1988) 53–64.

[11] R.A. Gingold, J.J. Monaghan, Smoothed particle hydrodynamics: theory and application to non-spherical stars, Mon. Not. Roy. Astron. Soc. 181 (1977) 375–389.

[12] R.A. Gingold, J.J. Monaghan, Kernel estimates as a basis for general particle methods in hydrodynamics, J. Comp. Phys. 46 (1982) 429–453.

[13] R. Glowinski, W.M. Lawton, M. Ravachol, E. Tenenbaum, Wavelets solution of linear and nonlinear elliptic, parabolic and hyperbolic problems in one space dimension, in: R. Glowinski, A. Lichnewsky (Eds.), Computing Methods in Applied Sciences and Engineering, SIAM, Philadelphia, 1990, pp. 55–120.

[14] F.C. Gunther, W.K. Liu, Implementation of boundary conditions for meshless methods, Comput. Meth. Appl. Mech. Eng. 163 (1998) 205–230.

[15] A.L. Gurson, Continuum theory of ductile rupture by void nucleation and growth: Part I – yield criteria and flow rules for porous ductile media, J. Eng. Mater. Technol. 99 (1977) 2–15.

[16] S. Hao, W. Brocks, J. Heerens, J. Hellmann, Simulation of 3-D ductile crack growth by the Gurson–Tvergaar–Needleman model, in: Proceedings, ECF11 Poitier (France) 1996.

[17] S. Hao, W.K. Liu, T. Belytschko, On the localization and damage induce crack presented in the ICES98 Atlanta, Published in Computational Mechanics, 1998.

[18] S. Hao, W.K. Liu, C.T. Chang, Computer implementation of damage models by finite element and meshfree methods, Comput. Meth. Appl. Mech. Eng., accepted.

[19] J.R. John, S.P. Shah, Mixed mode fracture of concrete subjected to impact loading, ASCE J. Struc. Eng. 116 (1990) 585–602.
[20] S. Jun, W.K. Liu, T. Belytschko, Explicit reproducing kernel particle methods for large deformation problems, Int. J. Numer. Meth. Eng. 41 (1998) 137–166.
[21] S. Li, W.K. Liu, Reproducing kernel hierarchical partition of unity Part II: applications, Int. J. Numer. Meth. Eng., accepted.
[22] W.K. Liu, An introduction to wavelet reproducing kernel particle methods, USACM Bull. 8 (1) (1995) 3–16.
[23] W.K. Liu, J. Adee, S. Jun, Reproducing kernel and wavelet particle methods for elastic and plastic problems, in: D.J. Benson, R.A. Asaro, (Eds.), Advanced Computational Methods for Material Modeling AMD 180 and PVP 268 ASME, 1993, pp. 175–190.
[24] W.K. Liu, C.T. Chang, Y. Chen, R.A. Uras, Multiresolution reproducing kernel particle methods in acoustic problems, Acoust. Vib. Rotating Mach. (ASME DE – Part B) 84 (2) (1995) 881–900.
[25] W.K. Liu, Y. Chen, Wavelet and multiple scale reproducing kernel methods, Int. J. Numer. Meth. Fluids 21 (1995) 901–935.
[26] W.K. Liu, S. Jun, Multiple scale reproducing kernel particle methods for large deformation problems, Int. J. Numer. Meth. Eng. 41 (1998) 1339–1362.
[27] W.K. Liu, S. Jun, S. Li, J. Adee, T. Belytschko, Reproducing kernel particle methods for structural dynamics, Int. J. Numer. Meth. Eng. 38 (1995) 1655–1679.
[28] W.K. Liu, S. Jun, Y.F. Zhang, Reproducing kernel particle methods, Int. J. Numer. Meth. Fluids 20 (1995) 1081–1106.
[29] W.K. Liu, S. Li, T. Belytschko, Moving least square kernel Galerkin method (I) methodology and convergence, Comput. Meth. Appl. Mech. Eng. 143 (1997) 113–154.
[30] W.K. Liu, C. Oberste-Brandenburg, Reproducing kernel and wavelet particle methods, in: J.P. Cusumano, C. Pierre, S.T. Wu (Eds.), Aerospace Structures: Nonlinear Dynamics and System Response, AD33 ASME, 1993, pp. 39–56.
[31] W.K. Liu, Y. Zhang, M.R. Ramirez, Multiple scale finite element methods, Int. J. Numer. Meth. Eng. Fluids 32 (1991) 969–990.
[32] L. Lucy, A numerical approach to testing the fission hypothesis, A. J. 82 (1977) 1013–1024.
[33] A. Needleman, Dynamic shear band development in plane strain, J. Appl. Mech. (1989) 1–9.
[34] A. Needleman, V. Tvergaard, An analysis of ductile rupture modes at a crack tip, J. Mech. Phys. Solids 35 (1987) 151–183.
[35] J.R. Rice, D.M. Tracey, On the ductile enlargement of voids in triaxial stress field, J. Mech. Phys. Solids 17 (1969) 201–217.
[36] C. Ruggieri, T.L. Panontin, R.H. Dodds Jr., Numerical modeling of ductile crack growth in 3-D using computational cell elements, Int. J. Fracture 82 (1996) 67–95.
[37] H.M. Shodja, T. Mura, W.K. Liu, Multiresolution analysis of a micromechanical model computational methods in micromechanics, in: S. Ghosh, M. Ostoja-Starzewski (Eds.), AMD 212/MD 62 ASME, 1995, pp. 33–54.
[38] G. Strang, Wavelets and dilation equations: a brief introduction, SIAM Rev. 31 (4) (1989) 614–627.
[39] V. Tvergaard, Influence of Voids on shear band instabilities under plane strain condition, Int. J. Fracture Mech. 17 (1981) 389–407.
[40] V. Tvergaard, A. Needleman, K.K. Lo, Flow localization in the plane strain tensile test, J. Mech. Phys. Solids (1984) 115–142.
[41] R.A. Uras, C.T. Chang, Y. Chen, W.K. Liu, Multiresolution reproducing kernel particle methods in acoustics, J. Comput. Acoust. 5 (1) (1997) 71–94.